INTERNATIONAL JOURNAL FOR NUMERICAL AND ANALYTICAL METHODS IN GEOMECHANICS
Int. J. Numer. Anal. Meth. Geomech., **22**, 721–748 (1998)

FUNDAMENTAL YET SIMPLIFIED MODEL FOR LIQUEFACTION INSTABILITY

CHANDRA S. DESAI*,†, INNJOON PARK‡ AND CHANGMING SHAO‡

Department of Civil Engineering and Engineering Mechanics, The University of Arizona, Tucson, Arizona 87521-0072, U.S.A

SUMMARY

A fundamental procedure is proposed for the identification of liquefaction in saturated soils based on the instability in the material's microstructure. The disturbed state concept (DSC) provides a unified constitutive model for the characterization of entire stress–strain behaviour under cyclic loading, and the values of disturbance at threshold states in the deforming microstructure provides the basis for the identification of liquefaction. The procedure is verified with respect to laboratory behaviour of two sands, saturated Ottawa and Reid Bedford. A mathematical analysis of the DSC constitutive matrix is also performed. Procedures for the application of the DSC for simplified analysis and design, and in finite element procedures are presented. It is believed that the proposed model can provide a fundamental yet simplified procedure for liquefaction analysis, and as a result, it is considered to be an improvement over the available empirical and energy-based procedures. © 1998 John Wiley & Sons, Ltd.

Key words: cyclic behaviour; saturated sands; disturbed state concept; liquefaction; post liquefaction; threshold transitions; laboratory tests; validations; mathematical analysis; computer implementation; application

INTRODUCTION

Relatively loose and saturated sands liquefy during earthquakes and strong ground motions. Such liquefaction can cause damage to foundations, buildings, earth retaining structures, dams, and other civil engineering structures. Observed and well-documented cases of the damage have been reported extensively, e.g., the Niigata, El Centro, Chile, Mexico, and more recently Kobe, Loma Prieta, and Northridge earthquakes.

The damage to property and life due to liquefaction has spurred considerable research activities over the last 30 years or so. Among the conventional and empirical procedures for the identification of liquefaction are the blow-count method, which is perhaps the oldest and often reliable, and those based on equivalent uniform shear stress and loading cycles on laboratory specimens under simulated cyclic loading.[1] An approach based on fundamental

* Corresponding author. Department of Civil Engineering and Engineering Mechanics, The University of Arizona, Tucson, Arizona, 87521-0072 U.S.A.
† Regents' Professor.
‡ Graduate Assistants.

Contract grant sponsor: National Science Foundation; contract grant number: CES 8711764; contract grant number: MSM 8618914

CCC 0363–9061/98/090721–28$17.50

Received 14 July 1997
Revised 24 November 1997

considerations related to accumulated or dissipated energy density during cyclic loading has been proposed.[2–4]

The importance of additional research in the areas of constitutive modelling for dynamic behaviour of (saturated) materials, instability and liquefaction, and post-liquefaction behaviour has been emphasized in the recent report by Bardet *et al.*[5]

A new method based on a unified constitutive modelling approach, called the disturbed state concept (DSC), for the cyclic behaviour of soils is presented in this paper. This approach is based on fundamental considerations, yet it can provide a simplified procedure for the identification of instability in the material's microstructure leading to liquefaction. It can be used for both practical analysis and design and in conjunction with computational (finite element) methods.

The DSC provides a model for the entire response including pre-liquefaction, liquefaction, and post-liquefaction behaviour. Here, the main attention is given to the liquefaction response, with a brief description of the post-liquefaction behaviour. A description of the DSC is provided and then details are given on the criteria for identification of liquefaction. The procedure is verified with respect to the laboratory behaviour of two sands: saturated Ottawa sand tested using the multiaxial loading device, and saturated Reid-bedford sand tested using a torsional shear device.[4] A mathematical analysis of the DSC constitutive matrix for identification of instability is presented. Recommendations are given regarding the application of the procedure for analysis and design, and implementation in computer (finite element) procedures.

REVIEW

In several investigations,[6–24] liquefaction has been studied experimentally (in the laboratory) and empirical criteria based on shear stress, threshold strains, initial effective overburden and number of cycles to liquefaction have been proposed. Casegrande[7] presented a critical review of the liquefaction phenomenon. Dobry *et al.*[11] proposed an alternative procedure based on magnitude of induced shear strains. Vaid and Thomas[22] performed experiments and analysed both the liquefaction and post-liquefaction responses of a saturated sand. An approach based on the damage parameter was proposed mainly for the estimation of pore water pressures by Finn and Bhatia[25] and Zienkiewicz *et al.*[26] Comprehensive reviews of liquefaction and related developments are available in References 1, 14 and 16.

Liquefaction criterion based on dissipated or accumulated energy during cyclic loading can provide a fundamental basis for the analysis of liquefaction compared to the previous empirical procedures. Nemat-Nasser and Shakooh,[2] Davis and Berrill,[3] Law *et al.*,[27] and Figueroa *et al.*[4] have proposed and used energy-based criteria for liquefaction. Recently, Chai and Romstad[28] have used a modified form of a model proposed by Coffin[29] and Manson[30] and by Park and Ang[31] to predict plastic strain energy capacity and cumulative damage in structures under seismic loading conditions. Such approaches can lead to computation of cycles to fatigue failure that may relate to instability. The application of such models is restricted essentially to one-dimensional idealizations, as they do not include multidimensional (stress and strain) effects that contribute to development and growth of disturbance (damage), leading to microstructure instability.[32] It has been shown that the DSC model provides improved characterization of microcracking, damage, and instability, and the previous models can be derived as special cases of the DSC.[32–34]

Many researchers have identified certain states during deformation of saturated sands and have employed them in developing understanding and criteria for liquefaction. The quasi-steady

state (QSS)[16,35,36] is often defined as a special case of phase transformation. At higher deformations, the sand approaches the steady state (SS) or the critical state[37] at which the material deforms continually at constant volume and shear stress for given initial mean pressure. Vucetic[23] analysed cyclic response and reported that when the threshold cyclic shear strain[11] is exceeded the microstructure of the soil is changed irreversibly, and the soil stiffness is changed permanently. Such states are unified in the proposed DSC model and are referred to as *threshold* transitions; these can include transition from contractive to dilative state, peak stress, initial liquefaction, final liquefaction, and residual (ultimate) conditions. Furthermore, the DSC can provide a fundamental and mechanistic basis for liquefaction, which is considered to be a generalized alternative to the energy approach.

MECHANICS OF LIQUEFACTION BEHAVIOUR

Conventionally, liquefaction defines the state during cyclic deformation when a (loose) saturated sand loses shear strength and behaves as a viscous liquid. During cyclic (earthquake) loading, liquefaction occurs as a consequence of the transfer of normal stresses on the soil grains to the pore water. Under the quick (undrained) loading conditions, the microstructure experiences strains at essentially constant volume. The level of pore water pressure during straining is controlled by the need to maintain constant volume by ensuring that the rebound of the soil skeleton during the reduction in effective stresses is sufficient to absorb the plastic deformations of the soil skeleton. The small compression of the water is neglected, but can be taken into account.[38] Finally, when the pore water pressure equals the normal stress, the shear strength of the soil is lost, as it acts like a *liquid*. As a result, the microstructure of the soil becomes unstable.

The disturbed state concept

This concept is based on the physical idea that the behaviour of a material mixture can be expressed in terms of the behaviour of its constituents. Depending upon the initial conditions (e.g., density and confining pressure), variation of material properties (inhomogeneity), geometry and loading conditions, the microstructure of the material element under cyclic loading may be considered to be composed of more than one material state. The internal self-adjustment of the microstructure can result in the development of clusters of particles with specific orientations that possess properties different from those of the material in the initial ('continuum') state, which is referred to as the relative intact (RI) state, Figure 1. The clusters, referred to as fully adjusted (FA) states, are the result of the self-organization of particles as affected by relative particle motions such as slippage, rotation, interpenetration and debonding between particles or a collection of particles, and microcracking and its coalescence. In this process, the initial RI material transforms continuously to the FA state, and, when the extent or volume of the FA part reaches critical or threshold states in the microstructure, instability and liquefaction can occur.

Under loading, the material can undergo localized (*unstable*) motions that may be called *local* instability involving oscillating motions of the particles, as shown schematically in Figure. 1. Here, (observed) deformations occur due to the self-adjustment of particles, so as to resist the external loading, and what is seen (or measured) at a point is the 'average' response for a group of particles around the point. The self-adjustment can lead to particle orientations that approach the

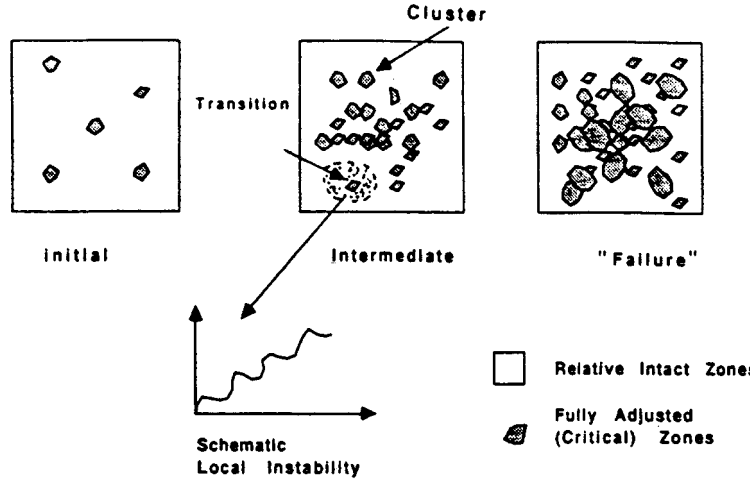

Figure 1. Relative intact and fully adjusted states in DSC, and local instability

FA state. Only when the extents of the FA zones reach certain values, threshold transitions can occur (see below).

Although a limited mathematical analysis of instability with respect to the properties of the DSC constitutive matrix is presented later, the foregoing definitions of threshold states are based on phenomenological considerations. Additional research will be needed to perform comprehensive mathematical analysis, with measurements of particle level responses within the material elements (specimens). An example of the latter is given in Figure 2.[39] It shows a vertical reconstruction using X-ray computerized tomography of a cylindrical specimen of a grout material tested under triaxial loading. The darker regions represent material parts that have approached the FA states in terms of the particle adjustments leading to clusters of density (void ratio). The threshold transitions at the point when contractive to dilative volume change and peak stress occur are found (for granular materials) around the disturbance $D(V^c/V)$ values of 0·15 and 0·20, respectively. Integration of the darker zones, Figure 2, yields the ratio of about 0·17. Thus, it is believed that similar and detailed measurements of internal particle configurations would lead to the validation of the idea of the decomposition of the deforming material in RI and FA parts in the DSC.

The self-organization of the clusters approach, asymptotically, the fully adjusted (FA) state, which can be characterized using the critical state concept.[33,37] The process of this transformation may involve 'locally' unstable motions; however, such motions by themselves may not cause global or macrolevel instability. Only when a large part (volume) of the RI material has transformed to the FA material may global instability occur. There can be more than one such threshold value of the volume of the FA material. For instance, a threshold value (D_v) of disturbance, D (= ratio of the volume in the FA state, V^c, to the total volume, V), is reached when the material experiences phase transformation (contractive to the dilative state). This state may, however, not cause global instability or liquefaction. However, when the value of D reaches the threshold, D_c (initial) liquefaction can occur, and when the material approaches the ultimate disturbance, D_u, Figure 3, *complete* collapse may occur. Somewhere between D_c and D_u, the final liquefaction may occur. From a practical viewpoint, the threshold state, D_c, is important when the

Figure 2. Vertical X-ray tomography reconstruction of grout specime under triaxial compression[39]

initial liquefaction occurs. The states, D_c, D_f and D_u can be measured in the laboratory; when the pore water pressure first equals the initial effective confining stress, when the pore pressure remains at the initial effective confining stress, and when the behaviour approaches the ultimate or residual state, respectively. However, the final state, when the entire material approaches the FA state ($D = 1$) when the RI material vanishes, is asymptotic and not measurable!

In the DSC, the observed behaviour (denoted by a) is considered to be due to the disturbance, with respect to the behaviour in the RI (denoted by i) and FA (denoted by c) states. It is expressed in terms of the behaviour in the RI and FA states by using the disturbance, D, which denotes the proportion of the volume of parts in the FA state with respect to the total volume of the material element, and acts as a coupling and interpolation (or extrapolation) mechanism. One of the important attributes of the DSC is that is allows for interacting mechanisms between the RI and

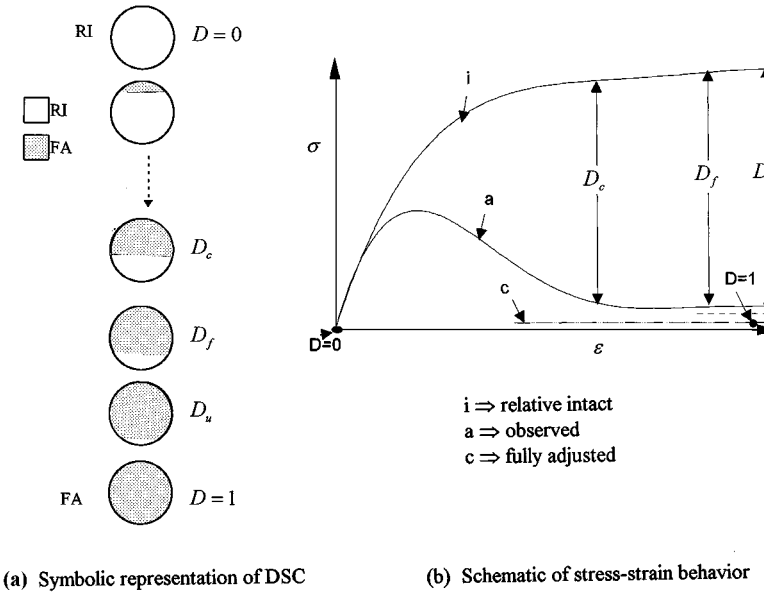

(a) Symbolic representation of DSC (b) Schematic of stress-strain behavior

Figure 3. Representations of DSC

FA parts, and hence, the microstructural changes are reflected in the observed behaviour. At the same time, the observed response is expressed in terms of the responses of the RI and FA parts, which can be measured (in the laboratory) based on macrolevel behaviour of finite-sized specimens. This is considered to be a distinct advantage over such other models as micromechanics, and microcrack interaction for which response at the particle level is required, which is difficult to measure. As a result, macrolevel response is used to define the microlevel behaviour in those models, which is a contradiction!

Furthermore, it may not be possible to develop a fundamental characterization of the global or macrolevel behaviour of a complex and non-linear (granular material) system by integrating the microlevel constitutive response from the behaviour of a few particles. For a consistent and fundamental characterization of such a granular material system containing millions of particles, it is essential to allow for the interacting mechanisms between its constituents. The self-organized criticality (SOC) concept[40] is based on the decomposition and interactions similar to those in the DSC. It may be noted that the SOC characterizes mainly the instability and catastrophic states, while the DSC allows for the entire stress–strain response including instability and liquefaction.

Disturbance function

The disturbance can be dependent on microstructural deformations (often defined as function of accumulated irreversible or plastic strains or dissipated energy), initial conditions (mean pressure, density), temperature, and moisture content. Usually, D is expressed as

$$D = \frac{V^c}{V} \tag{1}$$

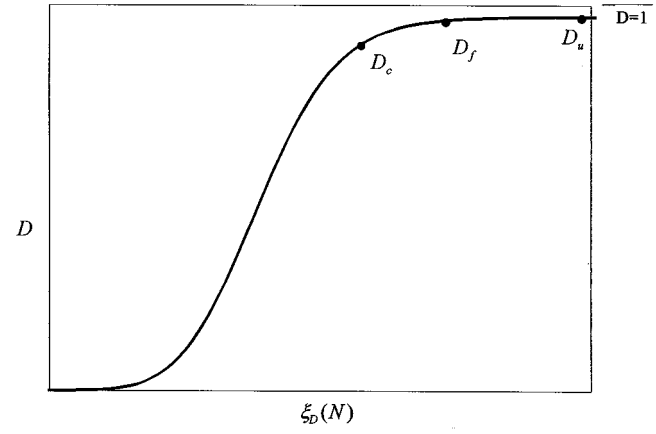

(a) Schematic of D vs ξ_D(N)

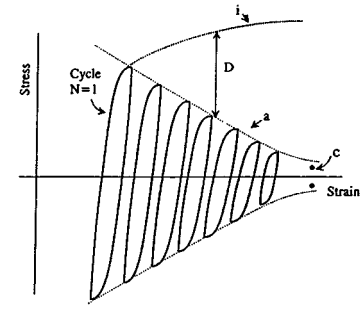

(b) Schematic of cyclic behavior and peak stresses

Figure 4. Disturbance function and cyclic behaviour

where V^{c} is the volume in the FA state and V is the volume of a material element. When the value of D reaches the threshold state, D_{c}, Figure 3 and 4, initial liquefication occurs, and when it reaches D_{f}, which is a state between D_{c} and D_{u}, final liquefaction occurs.

From experimental behaviour (see later descriptions), D can be expressed in terms of various measured quantities as

$$D_\sigma = \frac{\bar{\sigma}^{\mathrm{i}} - \bar{\sigma}^{\mathrm{a}}}{\bar{\sigma}^{\mathrm{i}} - \bar{\sigma}^{\mathrm{c}}} \tag{2a}$$

$$D_e = \frac{e^{\mathrm{i}} - e^{\mathrm{a}}}{e^{\mathrm{i}} - e^{\mathrm{c}}} \tag{2b}$$

$$D_{\sigma'} = \frac{\sigma'^{(\mathrm{i})} - \sigma'^{(\mathrm{a})}}{\sigma'^{(\mathrm{i})} - \sigma'^{(\mathrm{c})}} \tag{2c}$$

where $\bar{\sigma}$ is the measured stress such as $\sqrt{J_{2D}}$ (where J_{2D} is the second invariant of the deviatoric stress tensor, S_{ij}) or the principal stress difference ($\sigma_1 - \sigma_3$), or shear stress, τ; e is the void ratio, and σ' is the effective stress; the latter is used for undrained behaviour. D can also be defined based on non-destructive (ultrasonic) properties, e.g., velocity and attenuation.[34]

Assuming that the shear strains cause the predominant microstructural changes, D can be expressed in terms of the deviatoric plastic strain trajectory, ξ_D, as

$$D = D_u(1 - e^{-A\xi_D^Z}) \tag{3a}$$

where $D_u(< 1)$ is the ultimate or residual disturbance, Figure 3(b), ($D = 1$ is the asymptotic state and is not measurable in laboratory tests), A and Z are parameters that can be dependent on the initial pressure ($J_1'/3 = \sigma_o'$), initial density (ρ_0), number of cycles (N) and temperature:

$$\xi_D = \int [(d\underset{\sim}{E}^p)^T (d\underset{\sim}{E}^p)]^{1/2} \tag{3b}$$

in which $d\underset{\sim}{E}^p$ = vector of incremental deviatoric plastic strains. For cyclic loading, ξ_D is evaluated as function (N) based on the $d\underset{\sim}{E}^p$ corresponding to the peak stresses at different cycles. Then D is expressed as a function of N. Figure 4 shows the schematic of D as a function of $\xi_D(N)$.

The disturbance, D, Equation (3) can also be expressed in terms of dissipated (accumulated) energy, E, during the cyclic loading. In fact, as discussed later, use of both the plastic strain trajectory or the dissipated energy can lead to similar results. However, as laboratory and field data for dissipated energy are often not as readily available as the accumulated plastic strains, the latter can provide an easier approach.

DSC EQUATIONS

Based on the equilibrium forces in the observed, RI and FA states, the incremental constitutive equations to describe the observed response, Figure 3, are derived as[33,34]

$$d\underset{\sim}{\sigma}^a = (1 - D)\,\underset{\sim}{C}^i\, d\underset{\sim}{\varepsilon}^i + D\underset{\sim}{C}^c\, d\underset{\sim}{\varepsilon}^c + dD(\underset{\sim}{\sigma}^c - \underset{\sim}{\sigma}^i) \tag{4}$$

where $\underset{\sim}{\sigma}$ and $\underset{\sim}{\varepsilon}$ = vectors of effective stresses and strains, respectively; $\underset{\sim}{C}^i$ and $\underset{\sim}{C}^c$ are constitutive tensors for the RI and FA parts, respectively, d denotes increment, and dD is increment or rate of D. Here, the RI response ($\underset{\sim}{C}^i$) can be characterized by using models based on linear or non-linear elasticity, elastoplasticity, and thermoviscoplasticity.[32–34]

In the DSC, it is possible to use various assumptions regarding the strain increments in the observed ($d\underset{\sim}{\varepsilon}^a$), RI ($d\underset{\sim}{\varepsilon}^i$) and FA ($d\underset{\sim}{\varepsilon}^c$) states. If they are all different, relative motions can occur between the RI and FA states, and additional incremental strain equations are needed.[33] Then, iterative analysis needs to be performed in which initially the strain increments can be assumed to be the same, and then their different values are computed iteratively. If it is assumed that all the strains are equal, there occur no relative motions; this assumption can provide a simple method which is found to be appropriate for many problems. In the implementation of the DSC for dynamic analysis of porous media,[41] relative motions are permitted, e.g., see subsequent section on Computer Implementation.

The model in equation (4) provides a general framework for unified constitutive modelling,[33,34,42,43] as it includes various elasticity, plasticity, and damage models[44] as special cases. For example, if $D = 0$, equation (4) reduces to the incremental equations, $d\underset{\sim}{\sigma}^i = \underset{\sim}{C}^i\, d\underset{\sim}{\varepsilon}^i$, for

such continuum models, as the observed and intact responses are the same. It includes microcrack interaction effects implicity through second and third terms in equation (4), without the need for external imposition of microcrack interaction. Moreover, the DSC allows for, within its framework, ellipticity, characteristic dimension, localization, and avoids spurious mesh dependence. As a result, it does not need external enrichments such as gradient and Cosserat theories. Details of the foregoing aspects are presented in References 34, 45 and 46.

Post-liquefaction behaviour

The DSC model is capable of modelling the post-liquefaction behaviour, including the abrupt drop in the undrained strength. For example, it has been applied successfully to the thermomechanical behaviour of materials such as dislocated silicon crystals with oxygen impurities that exhibit an increase in the peak strength and stiffening after the softening.[47] One of the main reasons for this behaviour is that there occurs locking of dislocations due to the oxygen impurities. Although the microstructural changes due to reorientation of particles in a saturated soil that cause post-liquefaction stiffening may be different, the constitutive response is analogous to the behaviour of silicon.

Figure 5(a) shows a schematic of the response including peak, softening, and post-liquefaction stiffening. As indicated in Figure 5(b), the disturbance in the post-liquefaction region would decrease after the critical value of $\xi_D = \xi_D^p$. The disturbance function in Equation (3) is then modified as follows:

$$D = D_u^b[(1 - \exp(-A_b \cdot \xi_D^{Z_b}) - \bar{\lambda}(1 - \exp(-A_z \xi_D^{Z_h})] \tag{5}$$

where D_u^b, A_b and Z_b = parameters for the basic disturbance that defines softening, and $\bar{\lambda}$, A_z and Z_h = parameters to define the stiffening response. If the stiffening is not considered, only the first three parameters are required as in equation (3a). In equation (5), $\bar{\lambda}$ is given by

$$\bar{\lambda} = 0 \quad \text{if } \xi_D \leqslant \xi_D^p \tag{6a}$$

$$\bar{\lambda} = \frac{D_u^h}{D_u^b} \quad \text{if } \xi_D > \xi_D^p \tag{6b}$$

Then, the constitutive equation (4) are modified to include D in equation (5). Further research for this aspect is in progress.

Validations of the DSC model, equation (4), have been performed with respect to laboratory test results for a wide range of materials, sands,[48] clays,[43] ceramic-composites,[34] metal alloys[32] and stiffening in dislocated silicon.[47] The model is implemented in non-linear FE procedures for the solution of soil–structure interaction[49] and composites in electronic packaging.[50] In this paper, the main objective is to show the applicability of the approach for the characterization of liquefaction behaviour. At this time, it is achieved by the analysis of disturbance with respect to laboratory behaviour of saturated (Ottawa) sand,[51] and Reid-Bedford sand.[4]

ANALYSIS

The saturated Ottawa sand was tested using a multiaxial or truly triaxial device under cyclic stress-controlled loading with frequency $\omega = 0{\cdot}10$ Hz.[51] The tests were conducted with relative

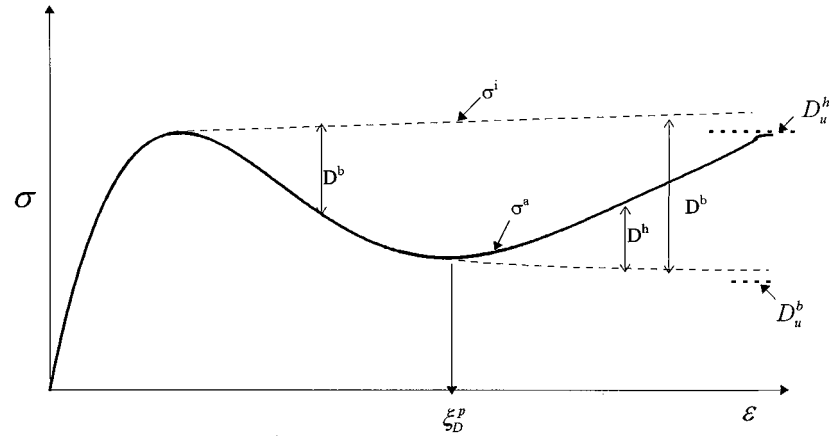

(a) Schematic of peak, softening, and stiffening response

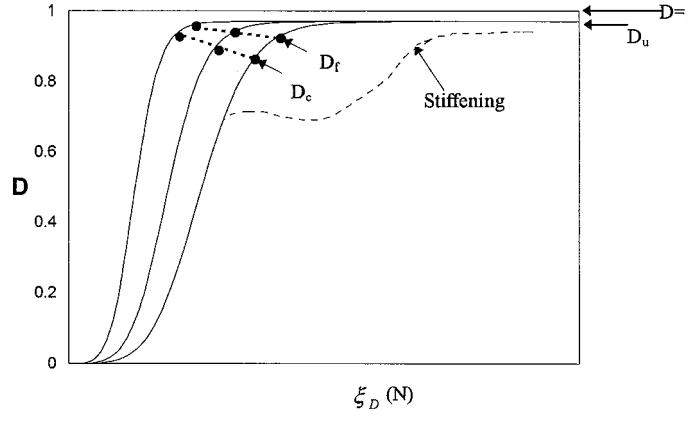

(b) Schematic of disturbance during softening and stiffening

Figure 5. Softening and stiffening behaviour, and disturbance

density, $D_r = 60$ per cent, and under three initial confining pressures, $\bar{\sigma}'_3 = 69$, 138, 207 kPa. Figures 6(a)–6(c) show the data for applied cyclic stress difference, measured axial strain (ε_z) and excess pore water pressure (Δu) vs. time for the three confining pressures. The stress difference ($\sigma_1 - \sigma_3$) vs. (ε_z) results are shown in Figures 7(a)–7(c). Plots of observed effective stress ($\bar{\sigma}' = J'_1/3$) were obtained from the results (Figures 6 and 7) and are shown in Figures 8(a)–8(c) for the three confining pressures.

The effective stress plots (Figure 8) were used to find the disturbance by using equation (2c), by employing the procedure described below to define the RI (i) response in Figure 8. Then the parameters A and Z were found by using equation (3). The value of D_u was adopted to be 0·99 as a simplification. It is possible to include different values of D_u based on residual

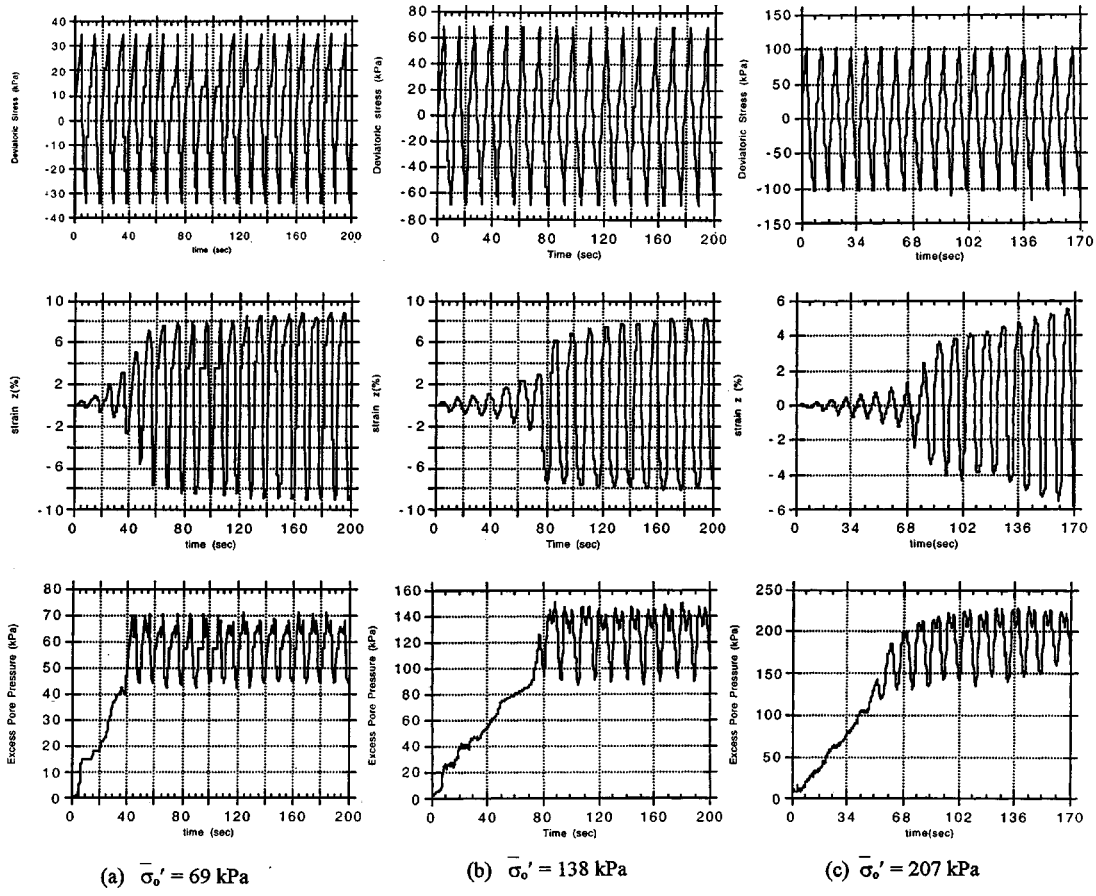

Figure 6. Stress, strain, pore water behaviour: Ottawa sand

stresses, particularly when such stress–strain curves are available (see Reid–Bedford sand example below).

Procedure for finding disturbance

In order to evaluate the disturbance, it is necessary to define the behaviour of the RI material, which can be characterized by using a continuum theory such as linear or non-linear elasticity and elastoplasticity. When the elastoplastic theory is used, the incremental stress–strain equations are expressed as

$$\mathrm{d}\underset{\sim}{\sigma}^{\mathrm{i}} = \underset{\sim}{C}^{\mathrm{ep(i)}}\ \mathrm{d}\underset{\sim}{\varepsilon}^{\mathrm{i}} \tag{7}$$

where $\underset{\sim}{\sigma}^{\mathrm{i}}$ and $\underset{\sim}{\varepsilon}^{\mathrm{i}}$ are the RI stress and strain vectors, and $\underset{\sim}{C}^{\mathrm{ep(i)}}$ is the elastoplastic constitutive matrix, which will depend upon the model used, e.g. von Mises, Mohr–Coulomb, critical state or

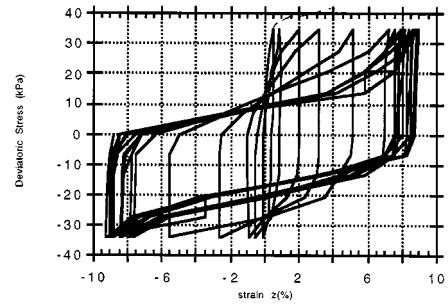

(a) $\bar{\sigma}_o' = 69$ kPa

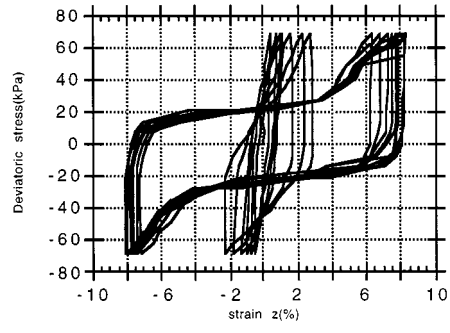

(b) $\bar{\sigma}_o' = 138$ kPa

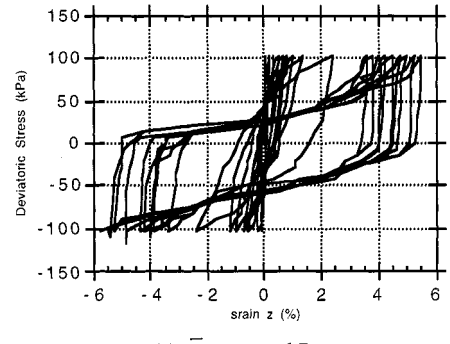

(c) $\bar{\sigma}_o' = 207$ kPa

Figure 7. Stress–strain behaviour: Ottawa sand

hierarchical single surface (HISS) plasticity.[33] Here, the HISS-δ_0 model is used in which the yield function, F, is given by

$$F = \bar{J}_{2D} - (-\alpha \bar{J}_1^n + \gamma \bar{J}_1^2)(1 - \beta S_r)^{-0\cdot5} = 0 \tag{8}$$

where the overbar denotes non-dimensionalized quantity with respect to the atmospheric pressure constant, p_a, S_r = stress ratio = $\sqrt{27}/2(J_{3D}J_{2D}^{-3/2})$, J_{3D} the third invariant of the deviatoric

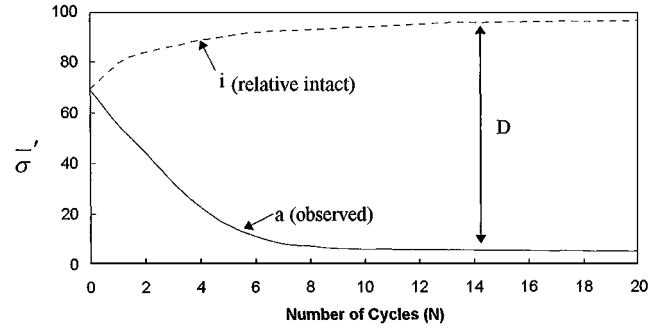

(a) $\overline{\sigma_o}' = 69kPa$

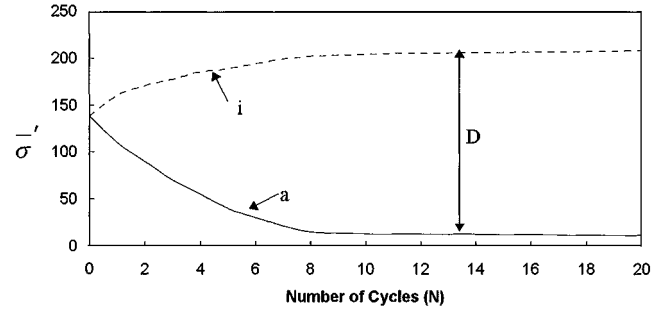

(b) $\overline{\sigma_o}' = 138kPa$

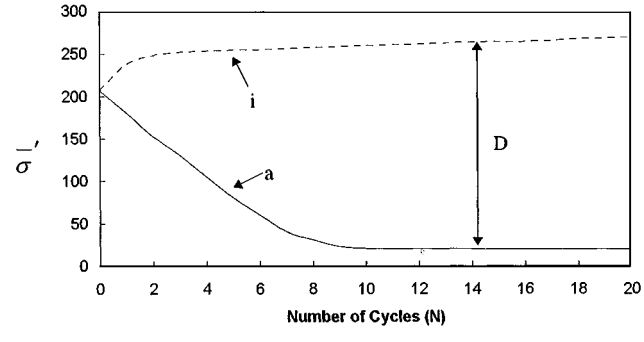

(c) $\overline{\sigma_o}' = 207kPa$

Figure 8. Observed and intact effective stress responses: Ottawa sand

stress tensor, S_{ij}, γ and β are the parameters related to the ultimate yield (or failure) behaviour and shape of yield surfaces, respectively, n is related to the transition from contractive to dilative state, and α is the hardening or growth function expressed as

$$\alpha = \frac{a_1}{\xi^{n_1}} \tag{9}$$

where a_1 and η_1 are the hardening parameters and ξ is the trajectory of plastic strains

$$= \int [(d\underset{\sim}{\varepsilon}^{\mathrm{p}})^{\mathrm{T}} (d\underset{\sim}{\varepsilon}^{\mathrm{p}})]^{1/2},$$

and $\varepsilon_{ij}^{\mathrm{p}}$ the plastic strain tensor.

It may be noted that equation (8) contains the classical plasticity (von Mises, Drucker–Prager), continuous yielding (critical state and cap) as special cases. Hence, although the above advanced (δ_0) model is used herein, one can adopt a simpler model to simulate the RI behaviour.

Disturbance

For the undrained behaviour under cyclic stress-controlled loading, the disturbance is found by using equation 2(c). Then, it is necessary to evaluate the effective stress, $\bar{\sigma}'$, for the RI behaviour. If the material did not experience microcracking and degradation, it can be assumed to continue to respond along the behaviour under the first cycle, Figure 7, for a given initial effective stress. This response can be treated as *relative* intact response. In fact, it is also possible to consider other RI responses such as linear elastic (based on the initial elastic moduli) and elastoperfectly plastic (based on the peak stress after the first cycle as the yield stress). Then the calculations of the RI effective stress ($\bar{\sigma}'$) can be performed as follows:

1. Integrate equation (7) for the RI response, say, by applying the strain increments corresponding to the cyclic behaviour, Figure 7. Here, the material parameters for the RI behaviour (δ_0-model) can be obtained from the first-cycle behaviour and monotonic (quasi-static) behaviour.
2. Compute the effective RI stress $\bar{\sigma}'^{(\mathrm{i})} = (\bar{\sigma}_1'^{(\mathrm{i})} + \bar{\sigma}_2'^{(\mathrm{i})} + \bar{\sigma}_3'^{(\mathrm{i})})/3$, where $\bar{\sigma}_{\mathrm{m}}'^{(\mathrm{i})} (m = 1, 2, 3)$ are the effective stress components. These are plotted in Figure 9 for the three confining stresses.
3. Plot $\bar{\sigma}'^{(\mathrm{i})}$ as shown in Figure 8 together with the observed effective stress, $\bar{\sigma}'^{(\mathrm{a})}$.
4. Assume that the effective stress, $\bar{\sigma}'^{(\mathrm{c})}$, at the FA state will be essentially zero.
5. Compute disturbance, D, as function of N, by using equation 2(c).

In the case of the strain-controlled tests, disturbance can be computed on the basis of the shear stress vs N response, subsequent Figure 15(a). Here, the RI response ($\bar{\sigma}^{\mathrm{i}}$) can be assumed to be that along the first cycle, the peak stresses at different cycles give the observed response ($\bar{\sigma}^{\mathrm{a}}$) and the asymptotic (ultimate) stress ($\bar{\sigma}^{\mathrm{c}}$) at higher cycles give the FA response. Then, equation (2a) is used to find the disturbance.

Fully adjusted state

The FA state can be characterized using different assumptions[33] that the FA material (1) has no strength at all like in the classical damage model,[44] (2) can carry hydrostatic stress but no shear stress, and (3) can carry the shear stress reached up to that state and deforms in shear at constant volume as in the critical state (CS) model.[37] It may be noted that there is a difference between the use of the CS in the DSC and the critical state soil mechanics. In the DSC, the CS is used for the FA material from the beginning of the loading as parts of the material

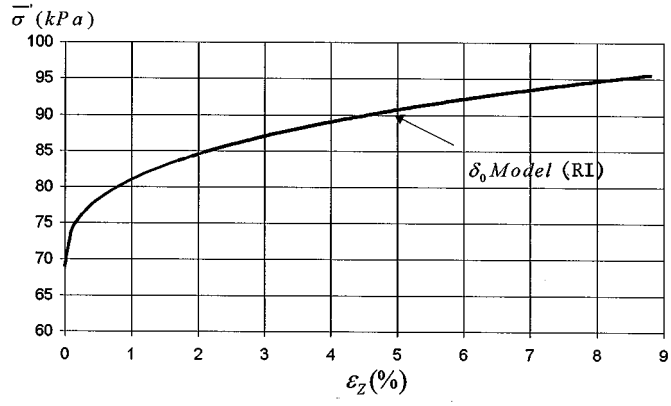

(a) $\bar{\sigma}_o' = 69$ kPa

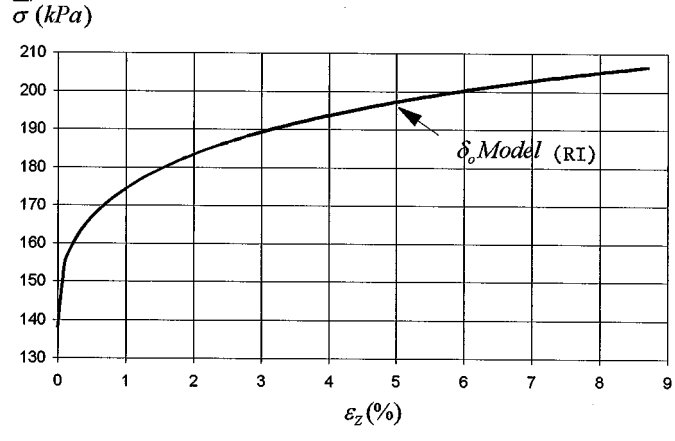

(b) $\bar{\sigma}_o' = 138$ kPa

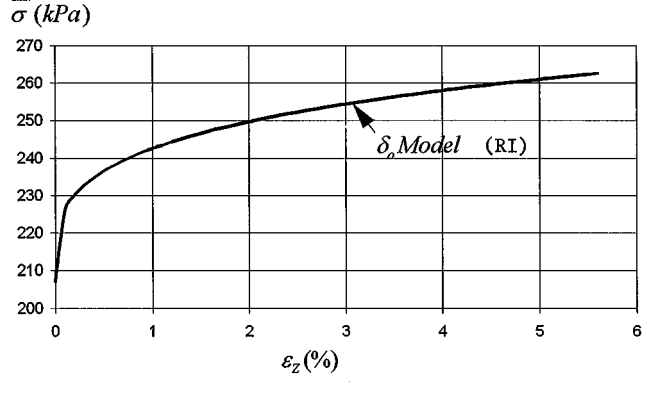

(c) $\bar{\sigma}_o' = 207$ kPa

Figure 9. RI effective stress vs axial strains: Ottawa sand

approach that state. Here, the FA behaviour, that is, matrix $\underset{\sim}{C}^{c}$ is defined by using the behaviour at the critical state:

$$\sqrt{J_{2D}}^{c} = mJ_1^c \tag{10a}$$

$$e^c = e_o^c - \lambda \ln(J_1^c/3p_a) \tag{10b}$$

where e_o^c = value of e^c for $J_1 = 3p_a$, and $\bar{m}$ and λ are the parameters.

Ottawa sand

The effective RI stresses ($\bar{\sigma}'$) for the Ottawa sand are calculated for the three confining stresses using the procedure described previously. They are plotted in Figure 9(a)–9(c), and also on Figures 8(a)–8(c) together with the observed effective stresses. Then the disturbances, D, are calculated by using equation 2(c), and are plotted on Figure 10(a)–12(a) for $\bar{\sigma}'_o = 69$, 138 an 207 kPa, respectively.

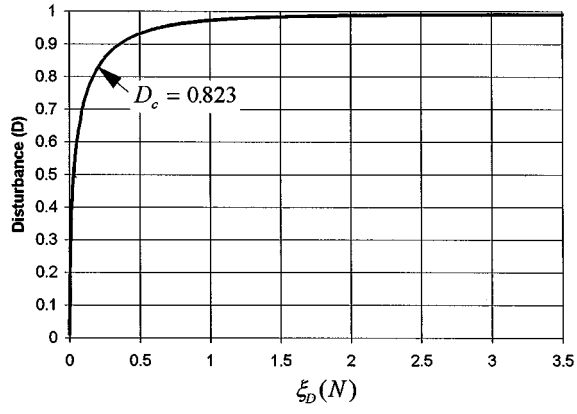

(a)

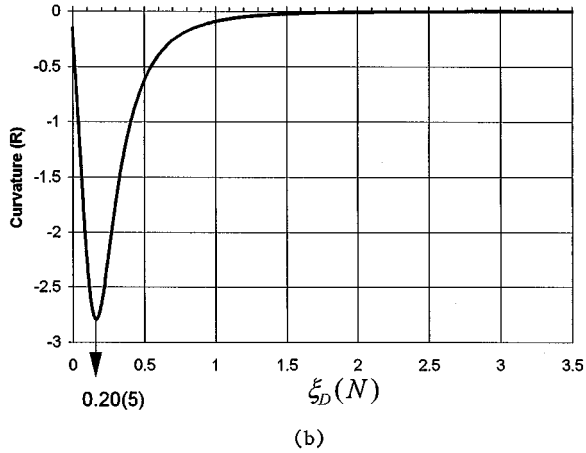

(b)

Figure 10. Disturbance and curvature vs deviatoric plastic strain trajectory as function of N, $\bar{\sigma}'_o = 69$ kPa; Ottawa sand

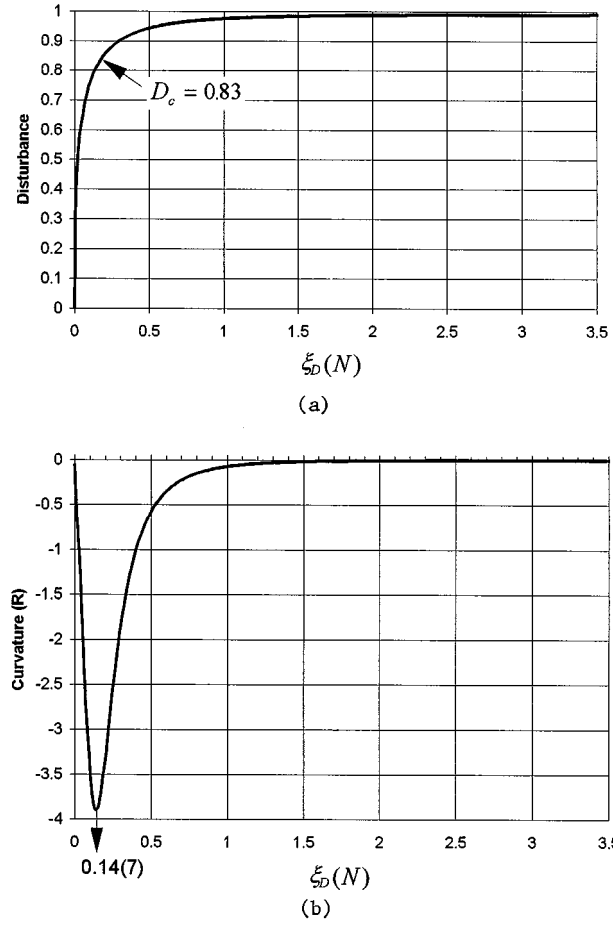

Figure 11. Disturbance and curvature vs deviatoric plastic strain trajectory as function of N, $\bar{\sigma}'_o = 138$ kPa; Ottawa sand

Instability and liquefaction

As can be seen in Figures 10(a)–12(a), a transition in the disturbance occurs when the curves stabilize towards the ultimate (FA) states. This transition occurs when the curvature (R) is minimum, which is defined as

$$R = \frac{D''}{(1 + D'^2)^{3/2}} \tag{10a}$$

where D' and D'' are the first and second derivations of D, equation (3)

$$D' = \frac{\mathrm{d}D}{\mathrm{d}\xi_D} = AZ\xi_D^{Z-1} - \exp(-A\xi_D^Z) \tag{10b}$$

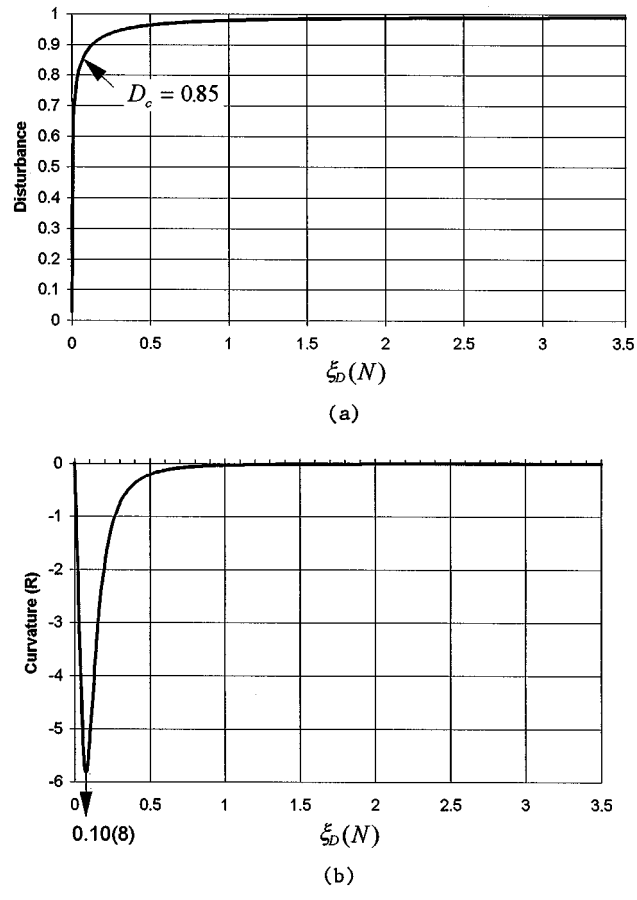

Figure 12. Disturbance and curvature vs deviatoric plastic strain trajectory as function of N, $\bar{\sigma}'_o = 207$ kPa; Ottawa sand

and

$$D'' = \frac{d^2D}{d\xi_D^2} = AZ\xi_D^{Z-2} \exp(-A\xi_D^Z)(Z - 1 - AZ\xi_D^Z) \tag{10c}$$

The solution of equation (10a) leads to the threshold value, D_c, at which the initial liquefaction occurs. Figures 10(b)–12(b) show the plots of R vs $\xi_D(N)$ together with the minimum states of R and the corresponding values of, ξ_D, and cycles, N_c, in parentheses. Tables I(a) and I(b) show the values of the parameters for the model, and Table I(c) shows the critical disturbance, D_c, and corresponding values of cycles, N_c, and ξ_D. It can be seen that the cycles $N_c = 5, 7$ and 8 corresponding to $D_c = 0{\cdot}82, 0{\cdot}83$ and $0{\cdot}85$, for the three initial confining pressures, compare well with those (about 5, 8 and 9 cycles) measured in the laboratory tests, Figure 6(a)–6(c), at which the excess pore pressure equalled the initial confining stress. Figure 13 shows the plot of N_c vs. $\bar{\sigma}'_o$, which can provide a basis for practical analysis (see below).

It can be seen from Table I and Figure 13 that the number of cycles to the initial liquefaction increases with $\bar{\sigma}'_o$. The values of ξ_D appear to decrease with $\bar{\sigma}'_o$, indicating that the extent of plastic

Table I. Parameters and results for Ottawa sand

(a) Elastic plastic (RI) and critical state (FA) models

Elastic:	$E = 193$ Mpa; $v = 0{\cdot}38$
Ultimate:	$\gamma = 1{\cdot}713$, $\beta = 0{\cdot}00$
Hardening:	$a_1 = 0{\cdot}845$; $\eta_1 = 0{\cdot}0215$, $n = 2{\cdot}45$
Critical State:	$\bar{m} = 0{\cdot}20$; $\lambda = 0{\cdot}019$, $e_o = 0{\cdot}593$

(b) Disturbance

$\bar{\sigma}'_o$ (kPa)	A	Z	D_u
69	3·98	0·51	0·99
138	4·20	0·47	0·99
207	4·48	0·31	0·99
Average	4·22	0·43	0·99

(c) Critical disturbance (D_c) and corresponding cycles (N_c) and ξ_D

$\bar{\sigma}'_o$ (kPa)	D_C	N_C	ξ_D
69	0·82	5	0·20
138	0·83	7	0·14
207	0·85	8	0·10
Average	0·83	7	0·15

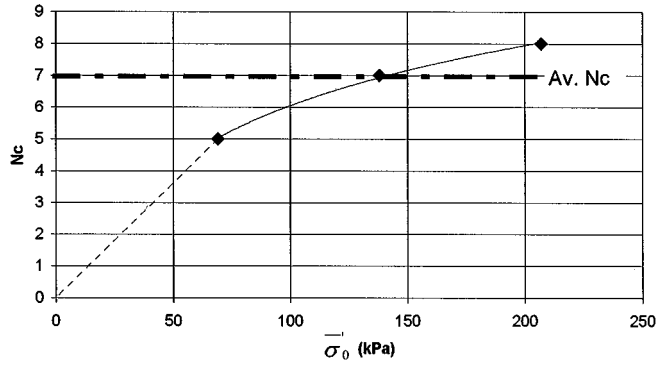

Figure 13. Initial effective confining stress vs number of cycles at critical disturbance

strains at liquefaction will be smaller for higher confining pressures. It is possible to identify final liquefaction using the DSC. However, the test results for the Ottawa sand from the stress-controlled tests were not sufficient for this evaluation. Hence, it is illustrated below with respect to torsional shear test data for the Reid–Bedford sand.

Reid–Bedford sand

Figueroa *et al.*[4] presented a series of cyclic shear tests for the Reid–Bedford sand (located south of Vicksburg, Mississippi), using the torsional device. The specimens were prepared at a relative density $D_r = 60$ per cent with initial mean pressure = 124·1 kPa. The tests were strain-controlled, with the amplitude of the shearing strain = 0·47 per cent. Figure 14 shows measured shear stress (τ) vs. shear strain. Figures 15(a) and 15(b) show the shear stress and pore water pressure vs. points (10 points/sec) during the cyclic loading.

The results in Figure 14 and 15(a) were used to compute the disturbance, D, using equation (2a). Here, the residual value of the shear stress $\cong$ 1·5 kPa, hence, the value of $D_u \cong 0{\cdot}967$. The plot of D vs N is shown in Figure 16(a), which shows that somewhere between cycles 9 and 11, the disturbance, D_c, is equal to about 0·87, when the curvature is the minimum. Then at the final liquefaction (cycles 14 to 16), the value of $D_f \cong 0{\cdot}920$. The ultimate disturbance, $D_u \cong 0{\cdot}967$, occurs when the shear stress stabilized toward a value equal to about 1·5 kPa, Figure 15(a). The value of D_f is midway between D_c and D_u. Thus, the predictions of the initial and final liquefaction from the DSC compare very well with the measured behavior, Figure 15(b), in which the initial liquefaction occurs between 9 and 11 cycles, and the final liquefaction between 14 and 16 cycles.

Figure 16(b) shows the plot of accumulated energy (E) during cyclic loading, Figure 14, vs cycles reported by Figueroa *et al.*[4] It can be seen that the plot of E vs. N and D vs. N, Figure 16(a) are similar. In other words, there can be identified threshold energy E_c and the state E_f corresponding to D_c and D_f. Thus, the DSC and energy approaches yield similar results.

Comments

There are a number of advantages of using the DSC compared to the energy approach, e.g., (1) the disturbance is a part of the constitutive model, equation (4), and allows characterization of the entire stress–strain response, while the energy approach allows for the identification of liquefaction, (2) the calculation of D is an integral part of the formulation and is available at every stage in the dynamic analysis, while separate calculations will be needed for the energy during the loading, (3) in the context of computer procedure, as D is available at every stage, its plots

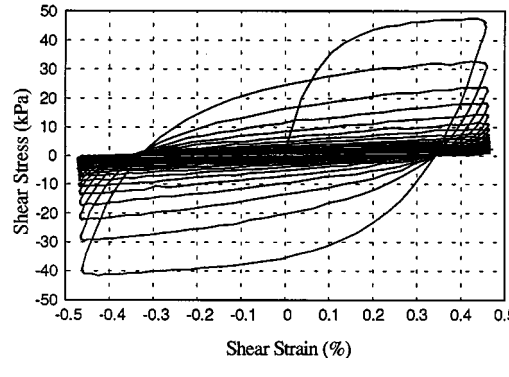

Figure 14. Shear stress vs strain response, Reid Bedford sand[4]

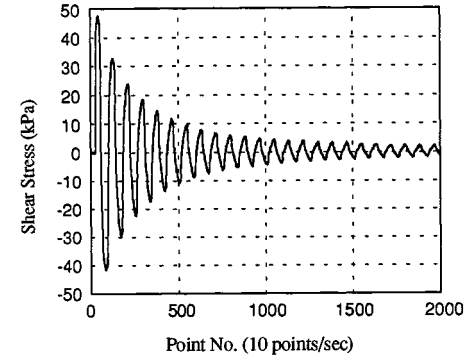

(a) Shear stress vs time

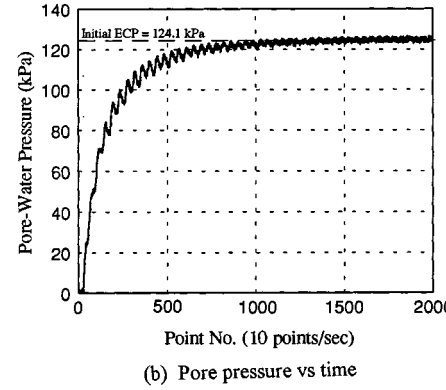

(b) Pore pressure vs time

Figure 15. Shear stress and pore water pressure vs. time: Reid Bedford sand[4]

(contours) can provide a complete and progressive picture of liquefaction zones in which D_c is reached and grows, and (4) the post-liquefaction stiffening response can also be characterized using the DSC.[47]

APPLICATIONS

The DSC model can be used for both practical analysis and design, and in computational procedures. Brief details of the proposed procedures are given below.

Laboratory behaviour

The procedures for the determination of D, based on laboratory test data, and identification of liquefaction, are outlined below:

1. Determine failure (or ultimate asymptotic) stresses from stress–strain data under at least three initial confining pressures, $(\bar{\sigma}'_o)$. Here, the stress–strain tests under monotonic loading can also be used.

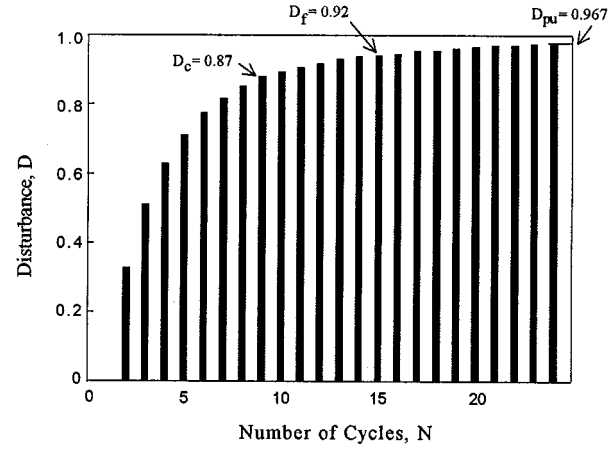

(a) Disturbance vs N

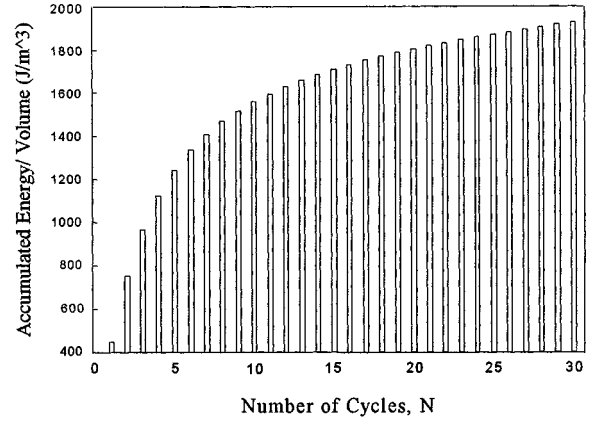

(b) Number of cycles, N (Figueroa et al. 1994)

Figure 16. Disturbance and accumulated energy: Reid Bedford sand

2. Use the first cycle of the stress–strain test, e.g. Figure 7, or shear stress vs. strain (or cycles) behaviour, Figures 14 and 15, to establish the RI behaviour. Here, the failure stress computed in step 1 is used to establish the ultimate yield stress for a given ($\bar{\sigma}'_0$). Now, the RI response can be simulated by using an advanced plasticity model such as the HISS-δ_0, or other suitable model. The latter can be non-linear elastic or elastoplastic model.
3. Compute the incremental and accumulated effective stresses using equation (7). This may be achieved manually or by preparing a computer routine for the integration of equation (7). Then evaluate the mean effective stresses, $\bar{\sigma}'$, for the RI behaviour, and plot them as on Figure 8.
4. For a simplified practical analysis, plot D vs. N for each confining pressure and locate the point of minimum curvature, which would denote initial liquefaction and the corresponding

cycle, N_c. Plot N_c vs. $\bar{\sigma}'$ (Figure 13), which can be expressed as

$$N_c = N_c(\bar{\sigma}'_o) \tag{11}$$

as a linear or non-linear function. This relation can be used to evaluate the number of cycles at which liquefaction would occur, depending upon the value of $\bar{\sigma}'_o$ in a soil deposit. As a simplication, an average value of N_c may be used.

Computer implementation

For computer implementation, it would be necessary to evaluate parameters D_u, A and Z for the disturbance function, equation (3), which is written as

$$Z \ln(\xi_D) + \ln(A) = \ln\left[-\ln\left(\frac{D_u - D}{D_u}\right)\right] \tag{12}$$

Here, ξ_D is found from the available stress–strain curves, Figures 7 and 14. The knowledge of the unloading modulus (E or G) allows computation of the increment of total strains, $d\underset{\sim}{\varepsilon}$, from which the deviatoric plastic strain increments are computed as

$$\mathrm{d}\underset{\sim}{E}^p = (\mathrm{d}\underset{\sim}{\varepsilon} - \mathrm{d}\underset{\sim}{\varepsilon}^e) - \tfrac{1}{3}\,\mathrm{d}\varepsilon_v^p\,\underset{\sim}{I} \tag{13}$$

where e denotes elastic, ε_v^p = plastic volumetric strain, and $\underset{\sim}{I}$ is unit matrix. A plot of $\ln(-\ln(1-D/D_u)$ vs. $\ln(\xi_D)$ provides the values of A and Z as the slope and the ordinate intercept, Figure 17. The value of D_u is computed from the residual stress [Figure 15(a)], using equation (2a); if such data are not available, it may be approximately assumed to be about 0·95.

Equation (4) can be expressed now in a simplified form as[33,45,50]

$$\begin{aligned}\mathrm{d}\underset{\sim}{\sigma}^a &= [(1-D)\,\underset{\sim}{C}^i + D\underset{\sim}{C}^c(1+\alpha) + R^T(\underset{\sim}{\sigma}^c - \underset{\sim}{\sigma}^i)]\,\mathrm{d}\underset{\sim}{\varepsilon}^i \\ &= \underset{\sim}{C}^{DSC}\,\mathrm{d}\underset{\sim}{\varepsilon}^i\end{aligned} \tag{14}$$

where $\underset{\sim}{C}^{DSC}$ is the DSC constitutive matrix, $\mathrm{d}\underset{\sim}{\varepsilon} = [1 + \bar{\alpha}(D)]\,\mathrm{d}\varepsilon^i$, $\bar{\alpha}(D)$ the relative motion parameter and $\underset{\sim}{R}$ is given by $\mathrm{d}D = \underset{\sim}{R}\,\mathrm{d}\underset{\sim}{\varepsilon}^i$. If $\bar{\alpha} = 0$, there is no relative motion between FA and RI parts, and the computations are simplified. Alternatively, an iterative analysis can be performed in which the starting value of $\bar{\alpha}$ is assumed to be zero, and then is progressively refined during increments and iterations. The resulting finite element equations are derived as

$$\int_V (\underset{\sim}{B}^T \underset{\sim}{L} \underset{\sim}{B}\,\mathrm{d}V)_{n-1}\,\mathrm{d}\underset{\sim}{q}_{i(n)} = \underset{\sim}{Q}_n - \int_V \underset{\sim}{B}^T \underset{\sim}{\sigma}^a_{n-1}\,\mathrm{d}V - \int_V (\underset{\sim}{B}^T \underset{\sim}{L}^r \underset{\sim}{R}\,\mathrm{d}V)\,\mathrm{d}\underset{\sim}{q}^i_{(n-1)} \tag{15}$$

where $\underset{\sim}{B}$ in the transformation matrix $\underset{\sim}{L} = (1-D)\,\underset{\sim}{C}^i + D(1+\alpha)\,\underset{\sim}{C}^c$, $\underset{\sim}{L}^r = (\underset{\sim}{\sigma}^c - \underset{\sim}{\sigma}^i)^T\,\underset{\sim}{R}$, $\underset{\sim}{Q}$ is the applied load vector, V denotes volume and n denotes increment.

Equations (15) denote implementation in the finite element procedure for dynamics of porous media based on the generalized Biot's theory.[41,52] Such a procedure allows calculation of disturbance at every stage of the dynamic loading, and the identification of the liquefaction zones when the threshold value, D_c, is reached.

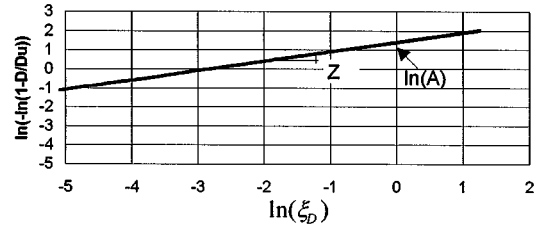

(a) $\bar{\sigma}_o' = 69$ kPa

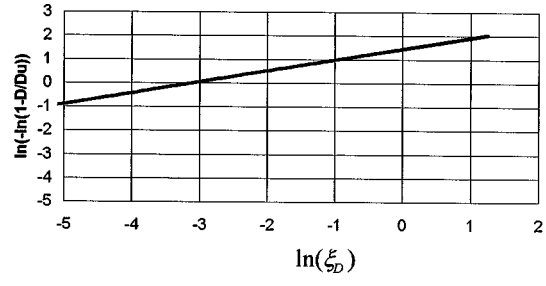

(b) $\bar{\sigma}_o' = 138$ kPa

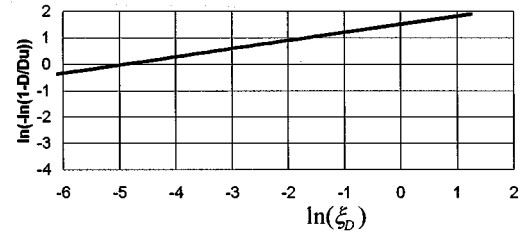

(c) $\bar{\sigma}_o' = 207$ kPa

Figure 17. Determination of disturbance parameters, Ottawa sand

Field applications

The DSC proposed here can be applied for field applications:

1. The procedure above, based on laboratory stress–strain behaviour, can be used for analysis of liquefaction in specific field soils tested.
2. A non-destructive procedure such as that based on ultrasonic measurements can be used to evaluate disturbance as[34]

$$D_V = \frac{V^i - V^a}{V^i - V^c} \tag{16}$$

where V is ultrasonic velocity. Then, D_V is correlated with D_σ to evaluate D_c that identifies liquefaction. This would require further research.

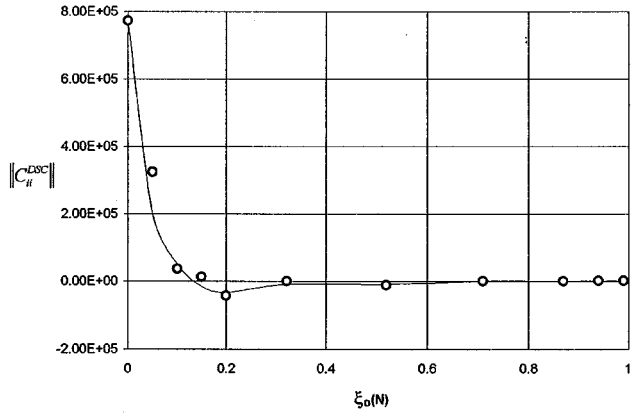

(a) $\bar{\sigma}_o' = 69$ kPa

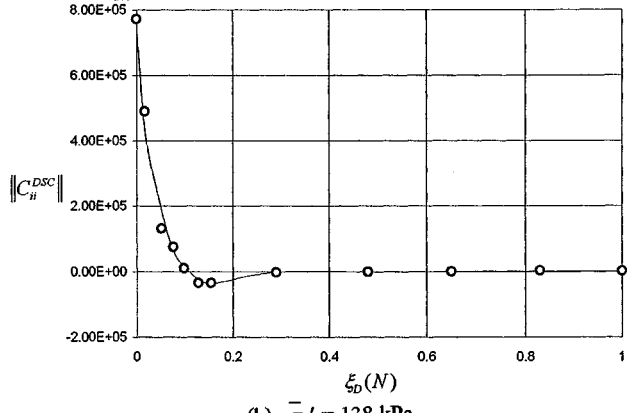

(b) $\bar{\sigma}_o' = 138$ kPa

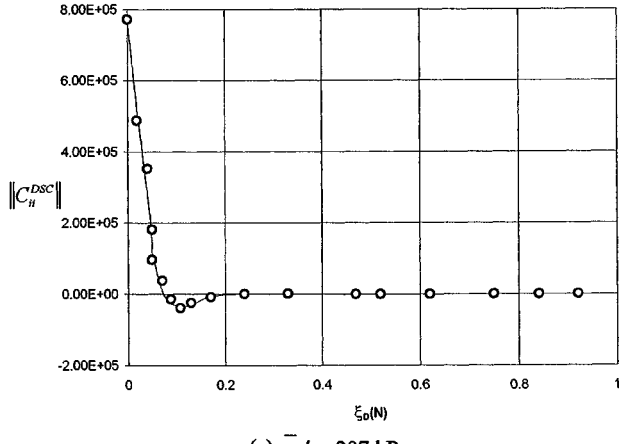

(c) $\bar{\sigma}_o' = 207$ kPa

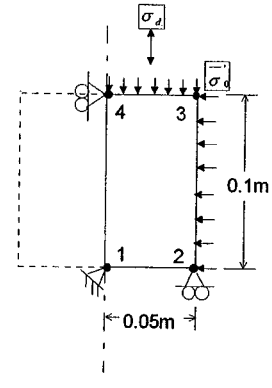

Figure 18. Plots of trace $\|C_{ii}^{DSC}\|$ vs. $\xi_D(N)$

3. Critical disturbance can also be found based on field vane shear tests based on plots of shear stress versus number of cycles. This would require additional research.
4. The finite element procedure can be used to perform comprehensive calculations of stress-deformation, pore water pressure and disturbance during dynamic loading for a given field problem. The plots of contours of D can then lead to zones where the critical disturbance is reached, signifying liquefaction.[52]

Mathematical analysis

In addition to the analysis and validations based on the test data, it is useful to perform mathematical analysis based on the properties of the constitutive matrix, $\underset{\sim}{C}^{\mathrm{DSC}}$, equation (14), and the stiffness matrix in equation (15). A limited analysis for the DSC model is described below.

Figure 18 shows a one-element mesh, idealized as axisymmetric, for the laboratory test behaviour of the Ottawa sand. In the finite element analysis, the initial pressures $\bar{\sigma}'_{\mathrm{o}} = 69$, 138 and 207 kPa are first applied, and then the cyclic stress-controlled loadings, Figure 6, are applied. Figures 18(a) to 18(c), show the variation of the trace of the matrix, $\|C_{ii}^{\mathrm{DSC}}\|$ vs. ξ_{D} as the function of number of cycles, N. The trace, which represents the sum of the eigenvalues, decreases, assumes a minimum value and then stabilizes to a small value as per equation (14), in the ultimate region when D approaches $D_{\mathrm{u}}(= 0{\cdot}99)$, and $\mathrm{d}D \approx 0$. The trace has minimum values at $\xi_{\mathrm{D}} \approx 0{\cdot}20$, $0{\cdot}15$ and $0{\cdot}10$, respectively, for $\bar{\sigma}'_{\mathrm{o}} = 69$, 138 and 207 kPa, respectively. These values correspond closely with the values at initial liquefaction corresponding to $D_{\mathrm{c}} = 0{\cdot}823$, $0{\cdot}830$ and $0{\cdot}850$ in Figures 10–12 at cycles to liquefaction, $N_{\mathrm{c}} = 5$, 7 and 8, respectively. Thus, the mathematical characteristics of the DSC correlate well with the initial liquefaction identified through critical values of D and the experimental behaviour of the sand.

CONCLUSIONS

A unified constitutive modelling approach based on the disturbed state concept (DSC) is used to characterize the cyclic response of soils and to define threshold states in the deforming microstructure. The threshold state, when the disturbance tends toward stabilization, leads to the critical disturbance, D_{c}, which identifies initial liquefaction. The final liquefaction occurs when the disturbance reaches a value of D_{f} between D_{c} and the ultimate disturbance, D_{u}. It is shown that D_{c} and D_{f} lead to cycles to liquefaction that compare very well with the laboratory observations on two saturated sands.

The results presented here involves effect of initial effective pressure for only one density, frequency of excitation and limited stress paths. Although they establish the validity of the DSC for liquefaction analysis, additional research would be required to analyse the effects of factors such as initial density, frequency and amplitude of loading and stress paths. Also, it would be desirable to develop procedures that can allow correlation between field and laboratory behaviour. For example, non-destructive testing techniques such as those using ultrasonic and Lamb waves can provide means to measure wave velocities that can be used to define the disturbance.[34]

The DSC can provide a fundamental procedure, which can be simplified for practical analysis and design, as well as for implementation in advanced computational (finite element) procedures. The approach allows calculation of D_{c} as an integral part of the procedure, leading to the identification and growth of liquefaction during dynamic (earthquake) loading. It is believed that

the proposed approach can provide a mechanistic, improved and simplified methodology for liquefaction analysis compared to the available empirical and energy-based procedures.

ACKNOWLEDGEMENTS

A part of the results presented herein were obtained under Grant Nos. CES 8711764 and MSM 8618914 from the National Science Foundation, Washington, DC. The tests for the Ottawa sand were performed by M.M. Gyi. Useful comments and suggestions by the reviewers, John Booker, J.T. Christian, R.O. Davis, W.D.L. Finn, Z. Mroz and J.M. Roesset, are gratefully acknowledged.

REFERENCES

1. National Research Council (NRC) 'Liquefaction of soils during earthquakes,' *Report No. CETS-EE001*, National Academic Press, Washington, DC, 1985.
2. S. Nemat-Nasser and A. Shokooh, 'A unified approach to densification and liquefaction of cohesionless sand in cyclic shearing,' *Can. Geotech. J.*, **16**(4), 659–678, (1979).
3. R. O. Davis and J. B. Berrill, 'Energy dissipation and seismic liquefaction in sands,' *Earthquake Engng. Struct. Dyn.*, **10**(1), 59–68 (1982).
4. J. L. Figueroa, A. S. Saada, L. Liang and N. M. Dahisaria, 'Evaluation of soil liquefaction by energy principles,' *J. Geotech. Engng., ASCE*, **120**(9), 1554–1569 (1994).
5. J. P. Bardet, I. M. Idriss, T. D. O'Rourke, N. Adachi, M. Aamada and K. Ishihara, *Proc., North America-Japan Workshop on Geotechnical Aspects of the Kobe, Loma Prieta and Northridge Earthquakes*, Osaka, Japan; University of California, Los Angeles, 1997.
6. K. Arulanandan and R. F. Scott (eds.) '*VELACS—Verification of Numerical Procedures for the Analysis of Soil-Liquefaction Problems*.' Vols. I & II, A. A. Balkema, Rottersdam, 1994.
7. A. Casagrande, 'Liquefaction and cyclic deformations of sands—a critical review,' *Harvard Soil Mech. Ser. No. 88*, Harvard University, Cambridge, Massachusetts, 1976.
8. G. Castro, 'Liquefaction of sands,' *Ph.D. Thesis*, Harvard University, Cambridge, MA, 1969.
9. G. Castro and S. J. Poulos, 'Factors affecting liquefaction and cyclic mobility,' *J. Geotech. Engng. ASCE*, **103**(76), 501–516 (1977).
10. J. T. Christian and W. F. Swiger, 'Statistics of liquefaction and S.P.T. results, *J. Geotech. Engng. Div. ASCE*, **101**(9), 1135–1150 (1975).
11. R. Dobry, R. S. Ladd, F. Y. Yokel, R. M. Chung and D. Powell, 'Prediction of pore water pressure buildup and liquefaction of sands during earthquakes by the cyclic strain method,' *Building Sciences Series 138*, National Bureau of Standards, Washington, DC, (1982).
12. W. D. L. Finn, P. L. Bransby and D. J. Pickering, 'Effect of strain history on liquefaction of sands,' *J. Soil Mech. Found. Div. ASCE*, **96**(6), 1917–1934 (1970).
13. W. D. L. Finn, 'Assessment of liquefaction potential and post liquefaction behavior of earth structures,' *Proc., 2nd Int. Conf. on Recent Advances in Geotech. Engng. and Soil Dynamics*, St. Louis, MO, II, 1991, pp. 1833–1851.
14. W. D. L. Finn, 'Evaluation of liquefaction potential,' State-of-the-Art Paper, *Proc. Int. Seminar on Soil Dynamics and Geotechnical Earthquake Engineering*, Lisbon, Portugal, 1992, p. 33.
15. I. M. Idriss and H. B. Seed, 'An analysis of ground motions during the 1957 San Francisco earthquake,' *Bull. Seismological Soc. Am.*, **58**(6), 2013–2932 (1968).
16. K. Ishihara, 'Liquefaction and flow failure during earthquakes,' *Geotechnique*, **43**(3), 351–415 (1993).
17. R. F. Scott and K. A. Zuckerman, 'Sandblows and liquefaction in the great Alaska earthquake of 1964,' *Eng. Pub. No. 1606*, Natl. Acad. Of Sciences, Washington, DC, 1972, pp. 170–189.
18. H. B. Seed, 'Soil liquefaction and cyclic mobility evaluation of level ground during earthquakes,' *J. Geotech. Engng. ASCE*, **105**(2), 201–255 (1979).
19. H. B. Seed and I. M. Idriss, 'Simplified procedure for evaluating soil liquefaction potential,' *J. Soil Mech. Found. Div., ASCE*, **97**(9), 1249–1274 (1971).
20. H. B. Seed and K. L. Lee, 'Liquefaction of saturated sands during cyclic loading,' *J. Soil Mech. Found. Engng. ASCE*, **92**(6), 105–134 (1966).
21. T. Shibata, H. Yukohomo and M. Miyoshi, 'Liquefaction process of sand during cyclic loading,' *Soils Found.*, **12**(1), 1–16 (1972).
22. Y. P. Vaid and J. Thomas, 'Liquefaction and post-liquefaction behavior of sand,' *J. Geotech. Engng. ASCE*, **121**(2), 163–173 (1995).
23. M. Vucetic, 'Cyclic threshold shear strains in soils,' *J. Geotech. Engng. ASCE*, **120**(12), 2208–2228 (1994).

24. T. Yamamoto, S. Ohara and M. Ishikawa, 'Liquefaction of saturated sand deposits under nonuniform vertical stresses,' *Tech. Report*, Faculty of Engng, Yamaguchi University, Japan, **5**(2)**,** 71–86 (1993).
25. W. D. L. Finn and S. K. Bhatia, 'Prediction of seismic pore water pressures,' *Proc. 10th Intl. Conf. on Soil Mech. and Found. Engineering*, Stockholm, Sweden, 3, 1981, pp. 201–206.
26. O. C. Zienkiewicz, K. H. Leung, E. Hinton and C. T. Chang, 'Liquefaction and permanent deformations under dynamic conditions—numerical solution and constitutive relations,' in: G. N. Pande and O. C. Zienkiewicz (eds), *Soil Mechanics — Transient and Cyclic Loads*, 1982, pp. 71–103.
27. K. T. Law, Y. L. Cao and G. N. He, 'An energy approach for assessing seismic liquefaction potential,' *Can. Geotech. J.*, **27,** 320–329 (1990).
28. Y. H. Chai and K. M. Romstad, 'Correlation between strain-based low-cycle fatigue and energy-based linear damage models,' *Earthquake Spectra*, **13**(2)**,** 191–209 (1997).
29. L. F. Jr. Coffin, 'A study of the effects of cyclic thermal stresses on a ductile metal,' *Trans. ASCE*, **76,** 931–950 (1954).
30. S. S. Manson, 'Behavior of materials under conditions of thermal stress,' *Report No. 1170*, National Advisory Commission on Aeronautics, Lewis Flight Propulsion Lab, Cleveland, Ohio, 1954.
31. Y. J. Park and A. H. S. Ang, 'Mechanistic seismic damage analysis of reinforced concrete,' *J. Struct. Engng. ASCE*, **111**(4)**,** 722–739 (1985).
32. C. S. Desai, J. Chia, T. Kundu and J. Prince, 'Thermomechanical response of materials and interfaces in electronic packaging, Part I—unified constitutive model; Part II—unified constitutive model, validation and design,' *J. Elect. Packaging ASME*, **119,** 294–309 (1996).
33. C. S. Desai, 'Constitutive modelling using the disturbed state as microstructure self-adjustment concept,' in: H. B. Mühlhaus (ed.), *Continuum Models for Materials with Microstructure*, Chapter 8, Wiley, France, 1995.
34. C. S. Desai and J. Toth, 'Disturbed state constitutive modelling based on stress-strain and nondestructive behaviour,' *Int. J. Solids Struct.*, **33**(11)**,** 1619–1650 (1996).
35. A. Alarcan-Guzman, G. A. Leonards and J. L. Chameau, 'Undrained monotonic and cyclic strengths of sands,' *J. Geotech. Engng. ASCE*, **114**(10)**,** 1089–1109 (1988).
36. K. Been and M. G. Jefferies, 'A state parameter for sands,' *Geotechnique*, **35**(2)**,** 99–112 (1985).
37. A. N. Schofield and C. P. Wroth, *Critical State Soil Mechanics*, McGraw-Hill, London, 1968.
38. G. R. Martin, W. D. L. Finn and H. B. Seed, 'Fundamentals of liquefaction under cyclic loading,' *J. Geotech. Engng., ASCE*, **101**(5)**,** 423–438 (1975).
39. C. W. Felice, V. J. Tester and J. Sharer, 'A Nondestructive Damage Assessment of PCGC Grout,' *Proc., Conf. on Containment of Underground Nuclear Explosions*, Univ. of Nevada, Reno, NV, U.S.A., 1991.
40. P. Bak and K. Chen, 'Self-organized criticality,' *Sci. American*, 26–33 (1991).
41. C. Shao, 'Implementation of DSC model for dynamic analysis of soil-structure interaction problems,' *Ph.D. Dissertation*, Dept. of Civil Engng. and Engng. Mechs., The Univ. of Arizona, Tucson, Arizona, 1997.
42. C. S. Desai and Y. Ma, 'Modelling of joints and interfaces using the disturbed state concept,' *Int. J. Numer. Anal. Meth. Geomech.*, **16**(7)**,** 623–653 (1992).
43. D. R. Katti and C. S. Desai, 'Modelling and testing of cohesive soil using the disturbed state concept,' *J. Engng. Mech., ASCE*, **121**(5)**,** 648–658 (1995).
44. L. M. Kachanov, Introduction to Continuum Damage Mechanics, Martinus Nijhuft Publishers, Dordrecht, The Netherlands, 1986.
45. C. S. Desai, C. Basaran and W. Zhang, 'Numerical algorithms and mesh dependence in the disturbed state concept,' *Int. J. Numer. Meth. Engng.*, **40**(10)**,** 3059–3083 (1996).
46. C. S. Desai and W. Zhang, 'Computational aspects of disturbed state constitutive models,' *Int. J. Comp. Meth. Appl. Mech. Engng.*, **151,** 361–376 (1998).
47. C. S. Desai, T. Dishongh and P. Deneke, 'Constitutive modelling for thermomechanical behavior of dislocated silicon with impurities,' *J. Appl. Phys.* (1997) submitted.
48. S. H. Armaleh and C. S. Desai, 'Modelling and testing of a cohesionless material using the disturbed state concept', *Int. J. Mech. Behavior Mater.*, **5**(3)**,** 279–295 (1994).
49. C. S. Desai, C. Shao and I. J. Park, 'Disturbed state modelling of cyclic behavior of soils and interfaces in dynamic soil–structure interaction,' *Proc., 9th Int. Conf. On Computer Methods and Adv. In Geomech.*, Wuhan, China, (1997).
50. C. Basaran, C. S. Desai and T. Kundu, 'Thermomechanical finite element analysis using the disturbed state concept,' *J. Elect. Packaging, ASME*, **120,** March 1998.
51. M. M. Gyi, 'Multiaxial cyclic testing of saturated Ottawa sand,' *M.S. Thesis*, Dept. of Civil Engng. and Engng. Mechs., The Univ. of Arizona, Tucson, Arizona, 1996.
52. I. J. Park and C. S. Desai, 'Analysis of liquefaction in pile foundations and shake table tests using the disturbed state concept,' *Report to NSF*, Dept. of Civil Engng. and Engng. Mechanics, The Univ. of Arizona, Tucson, AZ, U.S.A., 1997.

